Computational design of superhelices by local change of the intrinsic curvature

Pedro E. S. Silva[1][0000−0002−8783−8740], Maria Helena
Godinho[1][0000−0002−9760−5983], and Fernão Vístulo de
Abreu[2][0000−0003−0452−3493]

[1] NOVA University of Lisbon, 2829-516 Caparica, Portugal
`pess@fct.unl.pt, mhg@fct.unl.pt`
[2] University of Aveiro, 3810-193 Aveiro, Portugal
`fva@ua.pt`

Abstract Helices appear in nature at many scales, ranging from molecules to tendrils in plants. Organisms take advantage of the helical shape to fold, propel and assemble. For this reason, several applications in micro and nanorobotics, drug delivery and soft-electronics have been suggested. On the other hand, biomolecules can form complex tertiary structures made with helices to accomplish many different functions. A particular well-known case takes place during cell division when DNA, a double helix, is packaged into a super-helix — i.e., a helix made of helices — to prevent DNA entanglement. DNA super-helix formation requires auxiliary histone molecules, around which DNA is wrapped, in a "beads on a string" structure. The idea of creating superstructures from simple elastic filaments served as the inspiration to this work. Here we report a method to produce filaments with complex shapes by periodically creating strains along the ribbons. Filaments can gain helical shapes, and their helicity is ruled by the asymmetric contraction along the main axis. If the direction of the intrinsic curvature is locally changed, then a tertiary structure can result, similar to the DNA wrapped structure. In this process, auxiliary structures are not required and therefore new methodologies to shape filaments, of interest to nanotechnology and biomolecular science, are proposed.

Keywords: Tendril perversions · DNA folding · Design, synthesis and processing.

1   Introduction

In nature, a variety of ingenious mechanisms have been developed to fold, propel and assemble. Many of them use the ability to shape their structure in helical configurations [17]. For instance, *Erodium*, a flowering plant, uses a particular mechanism for disseminating its seeds. First, after flowering, the plant stores enough elastic energy in the fruits by creating a tension between awns and a surrounding tissue. After a given threshold, the tissue snaps and seeds are flung away from the plant. After reaching the ground, awns start a cycle of winding or

unwinding depending on humidity, coiling when drying and straightening when wetting. These movements help seeds to move on the surface until finding a position to open a hole into the soil [21,6].

In biochemistry, the helical shape is very common and can be arranged in very different structures to accomplish different functions. For instance, DNA is made of two intertwined helices, and collagen, of three intertwined helices [16,14]. Furthermore, single, double and triple helices can also gain different shapes, creating super-helices — helices built with helices [13]. Their different shapes are critical to healthy functioning. For instance, chromosome segregation during cellular division requires considerable packaging to avoid DNA entanglement, while during transcription a more stretched fold must give access to RNA polymerase enzymes.

These are certainly only two simple examples that show how controlling the helical shape of filaments can be of great importance at very different length scales and for different purposes. Controlling the shape of artificial elastic filaments should also be highly desirable given the broad potential applications in soft-electronics [10,5], micro and nanorobotics [11,9], healthcare [23,1], and explains surging recent interest and technical developments in this field [4].

Two main mechanisms have been proposed for producing helices. Snir and Kamien suggested that entropic forces could be responsible for the helical folding of molecular chains [20]. The main idea is that the helix shape creates an excluded volume to solute molecules. In crowded environments, this creates an asymmetry which renders the helical configuration more stable. This type of mechanism can play an important role in the cellular packed environments explaining aggregation, orientation and organisation of co-linear similar molecules or structures.

The former mechanism of helical formation requires the existence of a crowded environment. This is not always available, as happens when helices appear in the macroscopic world, as in the curling behaviour observed in tendrils. In this case, helices are formed when changes in the material produce asymmetric internal stresses which create a variety of deformations, as combinations of stretching, bending and torsion [7]. This phenomenon can be easily illustrated when one side of a ribbon is run over with a blade, stretching one side of the ribbon relatively to the other. This modification creates an intrinsic curvature, whose intensity is related to the final number of loops. If instead of ribbons, this type of asymmetric stresses occur in linear filaments, then buckling instabilities can generate a spontaneous instability that turns the filament into a helical shape [8,12].

The way the asymmetric stresses are created in a filament can vary. For instance, a stretched elastic band can be glued upon a relaxed band of the same material [12]. In micro and nanotechnology, the strategy consists in modulating the concentration and the crosslinking density of temperature-responsive polymers [24,18,19]. In nature, stresses originate from asymmetric cellular organisations. These can even evolve in time, depending on factors such as cellular and water concentration or cellular composition [2].

In this work, we were inspired by the complex tertiary structures observed in biomolecules. In particular, we were attracted by the creation of helices made of helices — called superhelices — and by the peculiar shape of chromatin that takes place when DNA is packed during cell division.

We will show how it is possible to use computational modelling and simulation to design structures with shapes similar to those found in DNA. It will also be shown that these computational approaches can serve multiple purposes, since they can provide insights for experimental exploration and discovery, and they can also work as validation for the explanation of experimental results.

This paper is organised as follows. In the next section, we will discuss the main mechanisms that will be used to shape structures. Afterwards, we will describe two computational experiments. In the first case, the idea was to explain how superhelices could be generated. In the second case, we used the same strategy to experimentally shape a polymeric fibre. In practice, many factors can contribute to the final shape of the filament. Through computational/theoretical modelling it is possible to explain how the final shape is actually obtained.

2   Theory and computational methodology

Coiling linear filaments or ribbons has been achieved by several groups by creating an asymmetry along the main axis (longitudinal direction) of the filament [22,18]. For instance, setting up a bi-layered strip with different initial strains produces a mismatch between the two layers [12]. Upon release, one layer contracts more than the other, creating an intrinsic curvature and forming an arc. The curvature can increase by increasing the layers mismatch and forming a ring. The higher the curvature the higher the number of loops and smaller the radius. These helical structures are twistless helices and would collapse in a ring upon release and only if they are held a distance apart, they can have a pitch.

Helical curves can be described by using the Frenet-Serret (FS) frame, $Q = [\mathbf{T}, \mathbf{N}, \mathbf{B}]$, where $\mathbf{T}$ and $\mathbf{N}$ are tangent and normal vectors and $\mathbf{B}$ is the binormal vector given by the cross product of $\mathbf{T}$ and $\mathbf{N}$. The evolution of the FS frame can be written in terms of the Darboux vector, $\mathbf{\Omega}$, by the set of continuous differential equations:

$$Q'_i = \mathbf{\Omega} \times Q_i, \tag{1}$$

where $\mathbf{\Omega} = \kappa \mathbf{B} \pm \tau \mathbf{T}$, κ is the curvature and τ is the torsion. Here the curvature to torsion ratio is constant, a necessary and sufficient condition to define a helix, according to Lancrets theorem. Left- (L) and right-handed (R) helices differ by having opposite signs in the torsion factor.

The evolution of the FS frame is only discontinuous at inversion points (perversions). From a previous analysis [18], the equation for the evolution of the FS frame can be modified to hold the changes introduced by different types of perversions. With the application of three transformations at the perversion point, Eq. 1 can be rewritten as:

$$Q'_i = (S\mathbf{\Omega}) \times (R_{\mathbf{\Omega},\alpha} R_{\mathbf{N},-2\theta} Q_i). \tag{2}$$

4 P. E. S. Silva, M. H. Godinho, F. V. de Abreu

where S changes the handedness of the helix, $S\mathbf{\Omega} = S(\kappa\mathbf{B} + \tau\mathbf{T}) = \kappa\mathbf{B} - \tau\mathbf{T}$, $R_{\mathbf{N},-2\theta}$ expresses a rotation of the FS frame around the normal, θ is the angle between the tangent and the twisting vector, and $R_{\mathbf{\Omega},\alpha}$ adds further twisting to the perversion. $\alpha = 0$ corresponds to the description of symmetric perversions as commonly found in plant tendrils and gift ribbons. Both helices have the same centre line. By contrast, when $\alpha = \pi$ the antisymmetric perversion causes centre lines to be apart by twice of the helical radius.

In this work, we will use only $\alpha = \pi$ perversions to shape fibres. This is because these perversions can occur at well defined (engineered) positions, whereas symmetric perversions occur spontaneously at positions that can depend on the boundary conditions, but also on the unwinding process, being more difficult to control.

The way we will produce structures with different shapes (our tertiary structures) consists on connecting helices with opposite handedness through antisymmetric perversions. Therefore, left (L) and right (R) helical segments — our building blocks — are juxtaposed. It will be assumed that all L (or R) segments have the same length, but the length of L segments is different from the length of R segments. Different shapes can be obtained because antisymmetric perversions introduce a turning angle, which relates to the helix length helix by, $L = \Theta\sqrt{(a^2 + b^2)}$. Here Θ is the total turning angle, a the helical radius and b the height of the helix. In this work, for simplicity, a and b for all helical segments and, therefore, all segments have the same κ and τ. Different shapes can be obtained by changing the length of the two types of helical segments, and in this way by changing Θ.

In the next section we will show results obtained by running simulations using the molecular dynamics simulator LAMMPS (Large-scale Atomic/Molecular Massively Parallel Simulator) [15,3]. Filaments are modelled by a set of beads arranged in a simple cubic lattice and connected to first and second neighbours by harmonic potentials, $V_{x_1,x_2} = k_h/2(l - l_{0,n})$, where k_h is the elastic constant, l is the distance between beads x_1 and x_2 and $l_{0,n}$ is the equilibrium bond distances ($l_{0,1} = \sigma$, for firsts neighbors and $l_{0,2} = \sqrt{2}\,\sigma$, for second neighbors). An intrinsic curvature is created by changing the equilibrium bond distances in one side of the rod. Then the pre-strain of the rod is becomes $\chi = (l'_{0,1} - l_{0,1})/l'_{0,1}$, where $l'_{0,1}$ is the modified equilibrium bond distance. Our simulations used a deterministic integration of the equations of motion using a NVE integrator (Verlet/Leap-frog method) to update beads positions and velocities on each time step (step size of $1 \times 10^{-3}\,\tau$).

3 Computer simulations and experimental validation

To analyse how antisymmetric perversions can be used to modulate the shape of linear structures, two studies were performed. In a first study, the analysis uses a theoretical description of curves with perversions using equations (1) and (2). Then computer simulations with LAAMPS were performed, which allow us to suggest that filaments with these types of shapes should be capable of
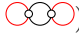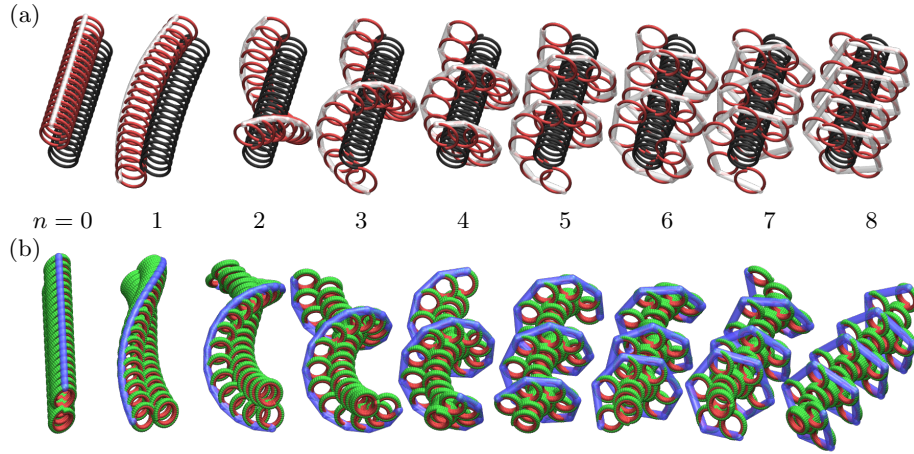
Figure 1. Filaments obtained from the juxtaposition of 20 R and 20 L helix segments (a) Shapes predicted with the theoretical model describing the evolution of the centre line according to equations (1) and (2) for helical segments with $\Theta_{\mathrm{R}} = 2\pi + \delta$ (represented in black) and $\Theta_{\mathrm{L}} = 2\pi$ (in red), and $\delta = 2\pi n/40$. (b) Computer simulations of filaments where the compression stresses (represented in red) act alternately on either side of the filament creating helices with antisymmetric perversions of $L_{\mathrm{R}} = (40+n)\ \sigma$ and with $L_{\mathrm{L}} = 40\ \sigma$.
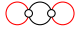.

being produced in practice. This is confirmed in our second study. There the same strategy to shape filaments is used on a polymeric fibre experimentally engineered to acquire a three-dimensional shape similar to those obtained in the previous study. In practice, the fibre obtained has a more complex shape, given the difficulties in controlling all experimental parameters, such as constant fibre thickness or equal building block lengths. Therefore, in a second stage of the study, we use the theoretical model to match the intrinsic curvature observed in the real fibre. This allows us to compare with the equivalent computer simulation.

3.1 Superhelices from helical blocks $\Theta_{\mathrm{R}} = 2\pi + \delta$ and $\Theta_{\mathrm{L}} = 2\pi$

The simplest (trivial) case considers R and L helical segments with the same length, i.e., with the same total turning angle, $\Theta_{\mathrm{R}} = \Theta_{\mathrm{L}}$. This case is shown in Fig. 1(a) $n = 0$, for $\Theta_{\mathrm{R}} = \Theta_{\mathrm{L}} = 2\pi$. Then each segment completes a full turn (2π), but as R and L helices - represented in red and black in Fig. 1(a) - have opposite handedness, every time one helix turns for one side, the following turns in the opposite direction. As a result, the full segment appears as it was made of two tied helices, united at the perversion points. The top view has the appearance ⭕✕⭕.

Keeping L helix blocks with exactly one loop, $\Theta_{\mathrm{L}} = 2\pi$, and slightly increasing the length of R helix blocks by δ, with $\delta = 2\pi n/40$ and $n = 1$ to 8, it can be

observed that the red (L) helix blocks start to revolve around of the black (R) helix blocks. Also, in these particular cases, where one block (red) has an integer number of loops, all other blocks (black) are aligned. The alignment occurs because only helix segment always completes a 2π turn, while the other revolves slightly more. Increasing n, increases the number of loops of the superhelix until $\delta = \pi$. Then, the black helix block have two side-by-side red helix blocks (top view: ⬭⬭). For $\delta > \pi$ the number of loops of the superhelix decreases until reaching an integer number of loops.

All these constructions were simulated for realistic elastic filaments by adjusting the curvature of one block with $L = 40\sigma$ to match one complete turn. Then, twenty R helix blocks with $L_R = (40 + n)$ σ alternated with twenty L helix blocks with $L_L = 40$ σ. When $n = 0$, the configuration matches the ⬭⬭ pattern predicted in Fig. 1(a) ($n = 0$).

For increasing n, rods develop a superhelix structure with an increasing number of turns. However, R helix blocks, which were aligned in Fig. 1(a), are now misaligned. This can be due to the fact that equation (2) describes the effect of the perversion in a simplified way, reducing its extent to a single point. In practice, perversions have an extension in which they deform the filament in a non-trivial way.

In any case, there is a good agreement in both approaches and, most importantly, in both approaches show that filaments with complex tertiary structures can be constructed using this simple strategy.

3.2   Designing Polymeric superhelices

The former analysis instigated us to produce experimentally a superhelix with a real polymeric fibre. A 4 cm long fibre was pre-strained to 9.15 cm and, then, irradiated for 5 h, on both sides with ultraviolet (UV) and using the mask shown in Fig. 2(a). The fibre obtained upon release is shown in Fig. 2(b). The fibre displayed loops in a clear helical disposition and with different handedness.

Afterwards, we used the theoretical model to match the polymeric fibre, Fig. 2(c). Gravity forces altered the total height of the polymeric fibre. The torsion of the theoretical helix was adjusted to match with the experimental fibre, despite the later having no intrinsic torsion.

Then, using the adjusted quantities of the theoretical model, a rod with seven L helix blocks of length $L_L = 15\sigma$ alternated with six R helix blocks of length $L_L = 135\sigma$, Fig. 2(d) and pre-strain $\chi = 0.23$. One end of the rod was kept fix and an additional gravity-like force was used in all atoms, in such a way that all are under the influence of the same force. Overall, by visual comparison of Fig. 2(b) and 2(d), rod and polymeric fibre have a similar design.

4   Conclusions

A new method for designing filaments with complex tertiary structures resembling those of DNA, was presented. Interestingly, the creation of these structures
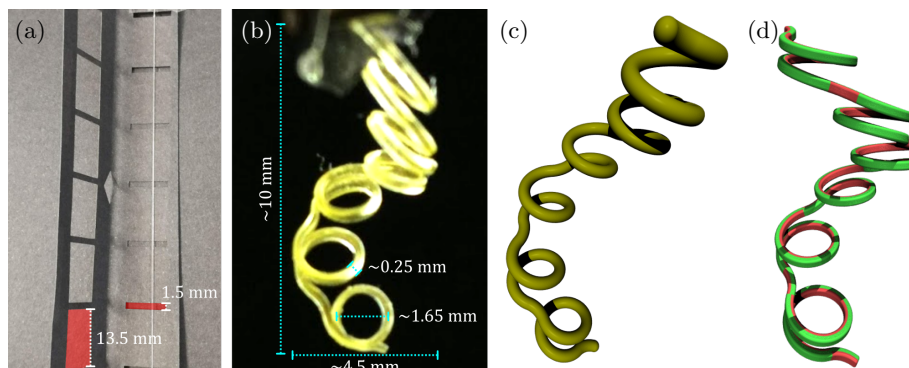
Figure 2. Filaments with seven L and six R helix blocks with 1:9 ratio. (a) Pre-strained polymeric fibre in a black cardboard mask before irradiation with UV light, in which different sides alternately cover the fibre with different region lengths. (b) Upon release, the polymeric fibre displays a superhelix shape. (c) Matching theoretical filament by adjusting with the experimental result. (d) Rod obtained by computer simulations of the theoretical model quantities.

does not require auxiliary structures to build up, as happens with histones in DNA. In this work, we also showed how a combination of analysis, in which computational and theoretical descriptions take an important part, help to build a thesis on how to design strategy to shape filament in effective ways. In particular, computational approaches offer a powerful tool to rapidly preview a given design.

Acknowledgement

References

1. An, B.W., Shin, J.H., Kim, S.Y., Kim, J., Ji, S., Park, J., Lee, Y., Jang, J., Park, Y.G., Cho, E., Jo, S., Park, J.U.: Smart Sensor Systems for Wearable Electronic Devices. Polymers **9**(12), 303 (Jul 2017). https://doi.org/10.3390/polym9080303
2. Armon, S., Efrati, E., Kupferman, R., Sharon, E.: Geometry and Mechanics in the Opening of Chiral Seed Pods. Science **333**(6050), 1726–1730 (Sep 2011). https://doi.org/10.1126/science.1203874
3. Brown, W.M., Wang, P., Plimpton, S.J., Tharrington, A.N.: Implementing molecular dynamics on hybrid high performance computers – short range forces. Computer Physics Communications **182**(4), 898–911 (Apr 2011). https://doi.org/10.1016/j.cpc.2010.12.021
4. Chen, Z., Huang, G., Trase, I., Han, X., Mei, Y.: Mechanical Self-Assembly of a Strain-Engineered Flexible Layer: Wrinkling, Rolling, and Twisting. Physical Review Applied **5**(1) (Jan 2016). https://doi.org/10.1103/PhysRevApplied.5.017001

5. Cheng, Y., Wang, R., Chan, K.H., Lu, X., Sun, J., Ho, G.W.: A Bio-mimetic Conductive Tendril for Ultrastretchable and Integratable Electronics, Muscles, and Sensors. ACS Nano **12**(4), 3898–3907 (Apr 2018). https://doi.org/10.1021/acsnano.8b01372

6. Evangelista, D., Hotton, S., Dumais, J.: The mechanics of explosive dispersal and self-burial in the seeds of the filaree, Erodium cicutarium (Geraniaceae). Journal of Experimental Biology **214**(4), 521–529 (Feb 2011). https://doi.org/10.1242/jeb.050567

7. Gerbode, S.J., Puzey, J.R., McCormick, A.G., Mahadevan, L.: How the Cucumber Tendril Coils and Overwinds. Science **337**(6098), 1087–1091 (Aug 2012). https://doi.org/10.1126/science.1223304

8. Goriely, A., Tabor, M.: Spontaneous Helix Hand Reversal and Tendril Perversion in Climbing Plants. Physical Review Letters **80**(7), 1564–1567 (Feb 1998). https://doi.org/10.1103/PhysRevLett.80.1564, goriely_spontaneous_1998

9. Hu, C., Pané, S., Nelson, B.J.: Soft Micro- and Nanorobotics. Annual Review of Control, Robotics, and Autonomous Systems **1**(1), 53–75 (May 2018). https://doi.org/10.1146/annurev-control-060117-104947

10. Jang, K.I., Chung, H.U., Xu, S., Jung, H.N., Yang, Y., Kwak, J.W., Jung, H.H., Song, J., Yang, C., Wang, A., Liu, Z., Lee, J.Y., Kim, B.H., Kim, J.H., Lee, J., Yu, Y., Kim, B.J., Jang, H., Yu, K.J., Kim, J., Lee, J.W., Jeong, J.W., Song, Y.M., Huang, Y., Zhang, Y., Rogers, J.A.: Self-assembled three dimensional network designs for soft electronics. Nature Communications **8**, 15894 (Jun 2017). https://doi.org/10.1038/ncomms15894

11. Lahikainen, M., Zeng, H., Priimagi, A.: Reconfigurable photoactuator through synergistic use of photochemical and photothermal effects. Nature Communications **9**(1) (Dec 2018). https://doi.org/10.1038/s41467-018-06647-7

12. Liu, J., Huang, J., Su, T., Bertoldi, K., Clarke, D.R.: Structural Transition from Helices to Hemihelices. PLOS ONE **9**(4), e93183 (2014). https://doi.org/10.1371/journal.pone.0093183

13. Main, E.R., Jackson, S.E., Regan, L.: The folding and design of repeat proteins: Reaching a consensus. Current Opinion in Structural Biology **13**(4), 482–489 (Aug 2003). https://doi.org/10.1016/S0959-440X(03)00105-2

14. Motooka, D., Kawahara, K., Nakamura, S., Doi, M., Nishi, Y., Nishiuchi, Y., Kang, Y.K., Nakazawa, T., Uchiyama, S., Yoshida, T., Ohkubo, T., Kobayashi, Y.: The triple helical structure and stability of collagen model peptide with 4(s)-hydroxyprolyl-pro-gly units. Peptide Science **98**(2), 111–121 (Jan 2012). https://doi.org/10.1002/bip.21730

15. Plimpton, S.: Fast Parallel Algorithms for Short-Range Molecular Dynamics. Journal of Computational Physics **117**(1), 1–19 (Mar 1995). https://doi.org/10.1006/jcph.1995.1039

16. Pusarla, R.H., Bhargava, P.: Histones in functional diversification. FEBS Journal **272**(20), 5149–5168 (Oct 2005). https://doi.org/10.1111/j.1742-4658.2005.04930.x

17. Silva, P.E.S., Vistulo de Abreu, F., Godinho, M.H.: Shaping helical electrospun filaments: A review. Soft Matter (2017). https://doi.org/10.1039/C7SM01280B

18. Silva, P.E.S., Trigueiros, J.L., Trindade, A.C., Simoes, R., Dias, R.G., Godinho, M.H., de Abreu, F.V.: Perversions with a twist. Scientific Reports **6**, 23413 (Mar 2016). https://doi.org/10.1038/srep23413

19. Silva, P.E.S., Godinho, M.H.: Helical Microfilaments with Alternating Imprinted Intrinsic Curvatures. Macromolecular Rapid Communications **38**(5), 1600700 (Mar 2017). https://doi.org/10.1002/marc.201600700

20. Snir, Y., Kamien, R.D.: Entropically Driven Helix Formation. Science **307**(5712), 1067–1067 (Feb 2005). https://doi.org/10.1126/science.1106243

21. Stamp, N.E.: Self-Burial Behaviour of Erodium Cicutarium Seeds. Journal of Ecology **72**(2), 611–620 (1984). https://doi.org/10.2307/2260070

22. Trindade, A.C., Canejo, J.a.P., Teixeira, P.I.C., Patricio, P., Godinho, M.H.: First Curl, Then Wrinkle. Macromolecular Rapid Communications **34**(20), 1618–1622 (Oct 2013). https://doi.org/10.1002/marc.201300436

23. Wolinsky, J.B., Colson, Y.L., Grinstaff, M.W.: Local drug delivery strategies for cancer treatment: Gels, nanoparticles, polymeric films, rods, and wafers. Journal of Controlled Release **159**(1), 14–26 (Apr 2012). https://doi.org/10.1016/j.jconrel.2011.11.031

24. Wu, Z.L., Moshe, M., Greener, J., Therien-Aubin, H., Nie, Z., Sharon, E., Kumacheva, E.: Three-dimensional shape transformations of hydrogel sheets induced by small-scale modulation of internal stresses. Nature Communications **4**, 1586 (Mar 2013). https://doi.org/10.1038/ncomms2549